Journal of Catalysis 280 (2011) 1–7

Contents lists available at ScienceDirect

Journal of Catalysis

journal homepage: www.elsevier.com/locate/jcat

Improvement of the photocatalytic hydrogen evolution activity of $Sm_2Ti_2S_2O_5$ under visible light by metal ion additives

Fuxiang Zhang [a], Kazuhiko Maeda [a,b], Tsuyoshi Takata [a], Kazunari Domen [a,*]

[a] Department of Chemical System Engineering, The University of Tokyo, 7-3-1 Hongo, Bunkyo-ku, Tokyo 113-8656, Japan
[b] Precursory Research for Embryonic Science and Technology (PRESTO), Japan Science and Technology Agency (JST), 4-1-8 Honcho Kawaguchi, Saitama 332-0012, Japan

ARTICLE INFO

Article history:
Received 14 November 2010
Revised 24 January 2011
Accepted 25 January 2011
Available online 3 March 2011

Keywords:
Hydrogen
Visible light
Modification
Photoelectrochemical
Water splitting

ABSTRACT

$Sm_2Ti_2S_2O_5$ was modified with various metal ions, and the effects on photocatalytic H_2 evolution from a Na_2S–Na_2SO_3 solution were investigated. In particular, the catalytic enhancement effects of magnesium and silver additives were focused on, and structural analysis and photoelectrochemical measurements were carried out to investigate the mechanism involved. It was found that their promotion effects were different. The addition of silver ions during the preparation of the photocatalyst resulted in the formation of Ag_2S nanoparticles and greatly promoted photooxidation of electron donors. Differently, the addition of magnesium ions significantly inhibited such photooxidation, but led to a reduction in the defect density in $Sm_2Ti_2S_2O_5$. The simultaneous addition of 5% Mg and 1% Ag was found to produce the highest level of catalytic performance. Finally, the optimal H_2 evolution rate of the modified photocatalysts reached 630 μmol h^{-1}, seven times that of an unmodified sample.

1. Introduction

There has recently been intense interest in the development of photocatalysts that can split water to produce hydrogen using only sunlight [1–4]. To date, more than 100 oxide-based photocatalysts have been explored, with some showing significant levels of photoactivity. However, the utilization of visible light on the oxide photocatalysts is restricted due to their wide band gaps [5].

A considerable amount of effort has been devoted to the development of water-splitting catalysts that are stable and sensitive to visible light. Many non-oxide materials, including metal (oxy)nitrides and oxysulfides, have been shown to be good candidates due to their stable H_2/O_2 half-reactions and efficient absorption in the visible region due to the substitution of O atoms with lower-negativity N or S atoms [6–17]. Among these non-oxide materials, the absorption edges of some compounds such as $LaTiO_2N$ [11], Ga–Zn–In mixed oxynitride [12], Ta_3N_5 [13,14], and $Sm_2Ti_2S_2O_5$ [15–17] can reach ca. 600 nm.

In addition to the exploration of new visible light-responsive materials, many innovative strategies have been developed to enhance the photocatalytic activity of existing candidate materials. This is more important for materials that absorb at wavelengths up to 600 nm, because the driving force on photogenerated carriers is much lower than that in wide band gap oxides. One common method of improving photocatalytic activity is to deposit a cocatalyst that allows more efficient separation of photogenerated electrons and holes [6,9,10,18–22]. Another important method of improvement involves modifying the photocatalyst with metal ions to adjust its local structure [23–26]. It is known that modification of a solid material with metal ions can modulate its physicochemical properties in a manner that depends on both the type of metal ions and the host material. One extensively studied example of this is the doping of TiO_2 photocatalysts with certain transition metals [27], rare earth metals [28], and noble metals [29], which results in enhanced photocatalytic activity. To the best of our knowledge, however, studies on metal-modified oxysulfides have been limited, because of the difficulty in controlling the preparation conditions for oxysulfides, especially in comparison with metal oxides.

Our earlier work revealed that $Sm_2Ti_2S_2O_5$ is a stable visible light-driven photocatalyst for H_2 and O_2 evolution, but its photocatalytic activity was very low [15]. Moreover, the preparation of $Sm_2Ti_2S_2O_5$ by solid state reaction not only required high temperatures over long period but also made it difficult to dope metals into the photocatalyst. To overcome these problems, we developed an H_2S gas sulfurization method for the preparation of fine $Sm_2Ti_2S_2O_5$ particles, which not only led to a large reduction in the preparation temperature and time but also allowed the possibility of metal doping [16]. Recently, we attempted to introduce Ag^+ ions into $Sm_2Ti_2S_2O_5$ prepared by the above-mentioned sulfurization method and achieved a remarkably enhanced H_2 evolution [17]. This result encouraged us to engage in a more systematic investigation.

In the present study, we examine the influence of various metal ion additives on the structure of the $Sm_2Ti_2S_2O_5$ phase and its H_2

* Corresponding author. Fax: +81 3 5841 8838.
E-mail address: domen@chemsys.t.u-tokyo.ac.jp (K. Domen).

0021-9517/$ - see front matter © 2011 Elsevier Inc. All rights reserved.
doi:10.1016/j.jcat.2011.01.027

evolution rate, along with the optimization of the preparation and experimental conditions of photocatalysts for H_2 evolution. Based on the experimental results, the effects of metal ion modification on photocatalytic activity are discussed. It was found that promotion of photocatalytic oxidation and reduction in defect density on the photocatalyst are two main factors of increasing photocatalytic H_2 evolution rate of $Sm_2Ti_2S_2O_5$.

2. Experimental

2.1. Preparation of photocatalysts

The synthesis of $Sm_2Ti_2S_2O_5$ photocatalysts with metal additives was similar to that described in our previous report [16]. Generally, it involved two steps: (i) synthesis of an amorphous oxide precursor by a polymerized complex method and (ii) sulfurization of the oxide precursor under an H_2S flow. All of the chemicals, which included $Sm(NO_3)_3{\cdot}6H_2O$ (Wako Pure Chemicals Co., 99.5%), $Mg(NO_3)_2{\cdot}6H_2O$ (Kanto Chemicals Co., 99%), $Ca(NO_3)_2{\cdot}4H_2O$ (Kanto Chemicals Co., 98.5%), $Sr(NO_3)_2$ (Kanto Chemicals Co., 99.5%), $Ba(NO_3)_2$ (Kanto Chemicals Co., 99%), $AgNO_3$ (Kanto Chemicals Co., 99.8%), $Cu(NO_3)_2{\cdot}3H_2O$ (Wako Pure Chemicals Co., 99.9%), $Zn(NO_3)_2{\cdot}6H_2O$ (Wako Pure Chemicals, 99%), $Y(NO_3)_3{\cdot}6H_2O$ (Kanto Chemicals Co., 99.99%), and $La(NO_3)_3{\cdot}6H_2O$ (Kanto Chemicals Co., 99%), were used without further purification.

The oxide precursor was typically synthesized as follows: 0.02 mol titanium tetraisopropoxide (Kanto Chemicals Co.) was dissolved in 0.2 mol ethylene glycol (Kanto Chemicals Co.) at room temperature, and 0.3 mol anhydrous citric acid (Wako Pure Chemicals) was then added and the mixture was heated at 333 K until it was completely dissolved. Subsequently, 0.02 mol $Sm(NO_3)_3{\cdot}6H_2O$, 20 mL methanol and a calculated amount of the metal additive precursor (the metal content was calculated according to the molar amount of Ti atoms) were added to the solution in that order. The mixture was stirred at 403 K until a transparent gel was formed. The polymer was carbonized at temperatures of 523, 573, and 623 K for 1 h each and finally calcined at 773 K for 12 h to completely remove the carbon.

The resulting amorphous oxide precursor was sulfurized at different temperatures (1073–1273 K) for 1 h under a flow of H_2S (10 mL min^{-1}). Post-calcination for 2 h in air at 573 K was then carried out to remove any sulfur species adsorbed on the surface of the photocatalyst [16]. A similar procedure was used to prepare the host $Sm_2Ti_2S_2O_5$ photocatalysts. In this paper, the as-prepared photocatalysts are denoted using the notation "A%M–$Sm_2Ti_2S_2O_5$-T" (A: metal content; M: metal; T: sulfurization temperature (K)).

2.2. Characterization of catalysts

The as-prepared samples were characterized by X-ray powder diffraction (XRD, Geiger-flex RAD-B, Rigaku; Cu Kα), field-emission scanning electron microscopy (FE-SEM; S-4700, Hitachi), ultraviolet–visible diffuse reflectance spectroscopy (JASCO, V-670 spectrophotometer), and X-ray photoelectron spectroscopy (XPS; JPS-9000, JEOL). The binding energies determined by XPS were corrected by reference to the C 1s peak (285 eV) for each sample. The Brunauer–Emmett–Teller (BET) surface area was measured at 77 K using a BELSORP-mini instrument (BEL Japan). Photoluminescence spectroscopy was measured at 77 K under 400 nm excitation using an FP-6600 instrument (Jasco).

2.3. Photocatalytic reactions

Reactions were carried out in a Pyrex inner irradiation-type reaction vessel connected to a glass closed gas circulation system. A 400 mL solution of 0.01–0.05 M Na_2S–Na_2SO_3 containing 0.2 g photocatalyst was used for H_2 evolution studies. A calculated amount of $RhCl_3{\cdot}xH_2O$ (Aldrich, 38–40%) precursor was added into the solution, which was photo-reduced into metallic Rh by the photogenerated electrons in the initial stage of photoreaction. The as-formed metallic Rh was well known to act as a cocatalyst for H_2 evolution in many references. The optimized 1 wt.% Rh was used in all the experiments. Prior to reaction, the solution was evacuated several times to completely remove any air and then irradiated with a 450 W high-pressure Hg lamp ($\lambda >$ 400 nm) using a 2 M $NaNO_2$ solution as an optical filter. A flow of cooling water was used to maintain the reactant solution at room temperature. The evolved gases were analyzed by gas chromatography. Unless specifically stated, 0.01 M Na_2S–Na_2SO_3 was used.

2.4. Measurement of apparent quantum efficiency

The apparent quantum efficiency was measured using a Pyrex top irradiation-type reaction vessel and a 300 W xenon lamp fitted with a 440 nm band-pass filter. Photoreduction of H^+ to H_2 was examined using an aqueous solution (200 mL) containing 0.20 g 1 wt.% Rh-loaded 1%Ag5%Mg–$Sm_2Ti_2S_2O_5$-1223 and 0.05 M Na_2S–Na_2SO_3 reagents. The number of photons reaching the solution was measured using a Si photodiode: the total incident photon rate at 440 nm was typically 1.71×10^{20} photons h^{-1}. The quantum efficiency was calculated using the following equation:

$$\Phi\ (\%) = (AR/I) \times 100 \quad (1)$$

where A, R, and I represent a coefficient (here, for H_2 evolution, $A = 2$), the H_2 evolution rate, and the rate of absorption of incident photons, respectively. Here, Φ corresponds to the apparent quantum efficiency. It was assumed that all incident photons were absorbed by the suspension.

2.5. Photoelectrochemical measurements

Photoelectrochemical measurements were taken using electrodes coated with a photocatalyst powder. The electrodes were prepared by pasting a viscous slurry onto a piece of conducting glass, following our previously reported procedure [17]. Typically, a mixture of 0.1 g of as-prepared powder, 10 μL of acetylacetone (Kanto Chemicals), 10 μL of Triton-X (Aldrich, USA), and 100 μL of distilled water was ground in an agate mortar to prepare the viscous slurry. This slurry was then pasted onto a fluorine-doped tin-oxide glass slide to produce a 1×3 cm^2 electrode, which was calcined in air at 573 K for 1 h before measurement.

Measurements were taken using a conventional Pyrex electrochemical cell, with a platinum wire counter electrode and an Ag/AgCl reference electrode under potentiostat control (HSV-100, Hokuto Denko, Japan). Current–voltage curves were measured in an aqueous solution of 0.01 M Na_2S–Na_2SO_3. The electrolyte solution was purged with nitrogen prior to the measurements and was maintained at room temperature by a flow of cooling water during the measurements. A 300 W xenon lamp with a wavelength of 420–800 nm was used as the light source.

3. Results and discussions

3.1. Effects of metal ion addition

Modification with 5 mol% alkaline earth metals (Mg, Ca, Sr, Ba) and transition metals (Ag, Cu, Zn, Y, La) was used to adjust the structure of $Sm_2Ti_2S_2O_5$ that was sulfurized at 1273 K for 1 h. Fig. 1 shows XRD patterns of the as-prepared samples, all of which indicate a single phase of $Sm_2Ti_2S_2O_5$ with no obvious peaks

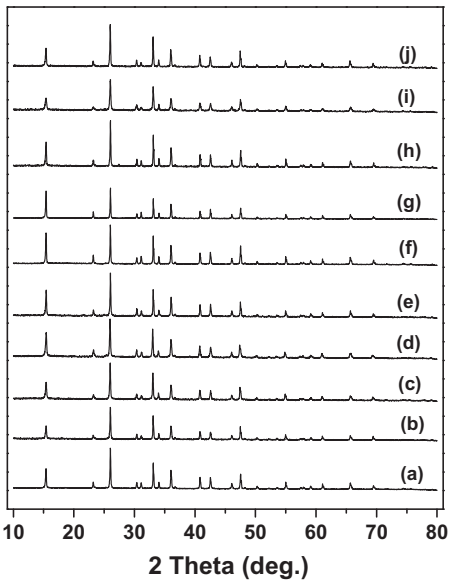

Fig. 1. XRD patterns of $Sm_2Ti_2S_2O_5$ with and without metal ion (5%) additives sulfurized at 1273 K for 1 h: (a) none, (b) Mg, (c) Ca, (d) Sr, (e) Ba, (f) Ag, (g) Cu, (h) Zn, (i) Y, and (j) La.

Table 1
Photocatalytic H_2 evolution rate[a] and BET data for various photocatalysts.

Entry	Photocatalysts	Radius of metal ions (pm)	Surface area ($m^2\ g^{-1}$)	H_2 rate ($\mu mol\ h^{-1}$)
1	$Sm_2Ti_2S_2O_5$-1273	–	7.2	85.7
2	5%Mg–$Sm_2Ti_2S_2O_5$-1273	86	7.2	253.2
3	5%Ca–$Sm_2Ti_2S_2O_5$-1273	114	7.0	172.6
4	5%Sr–$Sm_2Ti_2S_2O_5$-1273	132	6.6	92.4
5	5%Ba–$Sm_2Ti_2S_2O_5$-1273	149	3.0	36.8
6	5%Ag–$Sm_2Ti_2S_2O_5$-1273	129	6.7	143.6
7	5%Cu–$Sm_2Ti_2S_2O_5$-1273	91	4.6	30.3
8	5%Zn–$Sm_2Ti_2S_2O_5$-1273	88	5.5	98.6
9	5%Y–$Sm_2Ti_2S_2O_5$-1273	104	8.0	117.8
10	5%La–$Sm_2Ti_2S_2O_5$-1273	117.2	6.3	112.3

[a] Reaction conditions: catalyst, 0.2 g (1 wt.% Rh cocatalyst); aqueous Na_2S–Na_2SO_3 solution (400 mL); light source, 450-W Hg lamp with an $NaNO_2$ (2 M) solution filter ($\lambda > 400$ nm).

associated with the metal additives. This may be due to the low content of the metal species. Alternatively, they may form amorphous regions or become uniformly incorporated into the photocatalyst structure. The similar peak intensities and widths also indicate that the metal ion additives did not significantly affect the structure of the $Sm_2Ti_2S_2O_5$.

Fig. 2 shows that in most cases, the morphologies of the samples with and without metal additives were plate-like with smooth surfaces, except that the particles in the samples modified with 5% Ba or Cu were significantly larger. The primary particle size of $Sm_2Ti_2S_2O_5$ was 0.1–0.4 μm, but the extent of aggregation into secondary particles depended on the additive. The Zn- or La-modified samples exhibited much more pronounced aggregation. Compared with the parent $Sm_2Ti_2S_2O_5$ sample, the increase in primary particle size and the aggregation into secondary particles were probably responsible for the obvious decrease in the surface area of Ba-, Zn-, La-, and Cu-modified samples.

Table 1 compares the rate of H_2 evolution from 0.01 M Na_2S–Na_2SO_3 solution under visible light (>400 nm). Most of the metal additives other than Ba or Cu ions promoted H_2 evolution, to different extents. For the alkaline earth metal-modified samples, the larger the ionic radius of the metal, the lower will be the H_2 evolution rate. A 5%Mg-modified sample was found to show the highest activity. As for the other samples, the optimal H_2 evolution activity was obtained from the 5%Ag–$Sm_2Ti_2S_2O_5$-1273 sample.

A lower surface area can lead to lower photocatalytic activity, because of the decrease in the density of available reaction sites. However, in the present study, although the metal modification led to a decrease in surface area, it also promoted H_2 evolution, except for the case of Cu and Ba. This suggests that the metal additives probably affect the local surface or intrinsic structure of the photocatalyst, thereby enhancing the H_2 evolution activity. In order to better understand the promotional effect of metal modification, Mg- and Ag-modified samples, which demonstrated higher H_2 evolution rate, were characterized in more detail, as discussed in the following sections.

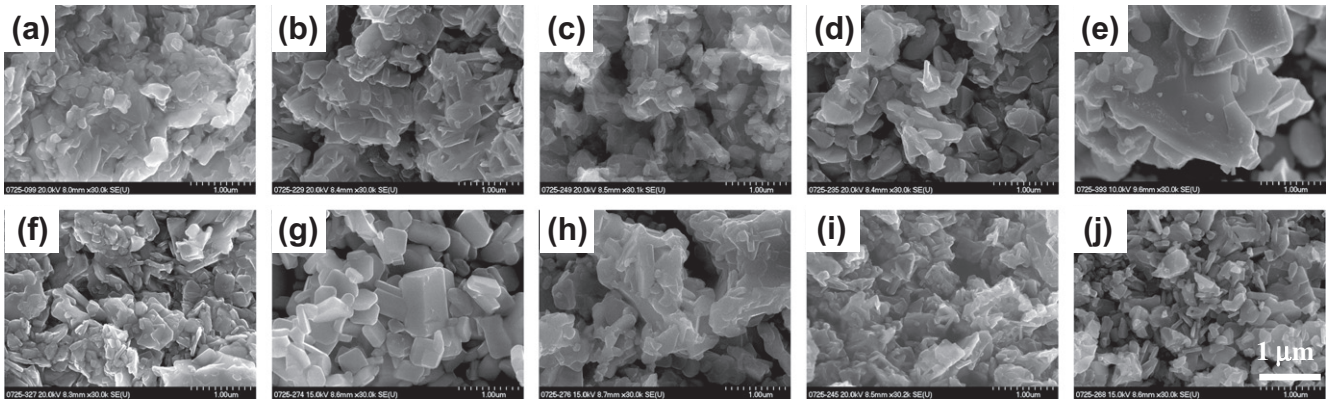

Fig. 2. Typical SEM images and BET data for metal (5%)-modified $Sm_2Ti_2S_2O_5$ samples sulfurized at 1273 K for 1 h: (a) none (7.2 $m^2\ g^{-1}$), (b) Mg (7.2 $m^2\ g^{-1}$), (c) Ca (7.0 $m^2\ g^{-1}$), (d) Sr (6.6 $m^2\ g^{-1}$), (e) Ba (3.0 $m^2\ g^{-1}$), (f) Ag (6.7 $m^2\ g^{-1}$), (g) Cu (4.6 $m^2\ g^{-1}$), (h) Zn (5.5 $m^2\ g^{-1}$), (i) Y (8.0 $m^2\ g^{-1}$), and (j) La (6.3 $m^2\ g^{-1}$).

Table 2
Effect of silver or magnesium content on the photocatalytic H_2 evolution rate.[a]

Content of Ag (mol%)	H_2 rate (μmol h^{-1})	Content of Mg (mol%)	H_2 rate (μmol h^{-1})
0	85.7	0	85.7
0.5	194.8	1	149.8
1	265.0	3	189.4
1.5	228.0	5	253.2
2.5	183.0	7	228.3
5	143.6	9	142.3
7.5	106.8		

[a] Reaction conditions: catalyst, 0.2 g (1 wt.% Rh cocatalyst); aqueous Na_2S–Na_2SO_3 solution (400 mL); light source, 450-W Hg lamp with an $NaNO_2$ (2 M) solution filter ($\lambda > 400$ nm). Photocatalysts were sulfurized at 1273 K for 1 h.

3.2. Magnesium- and/or silver-modified systems

3.2.1. Photocatalytic performances

The H_2 evolution rates of Mg- and Ag-modified samples were first optimized by adjusting the preparation and reaction conditions. Table 2 shows the H_2 evolution rates of photocatalysts with different metal additive content. The optimal Mg and Ag contents were found to be 5% and 1%, respectively. Based on the XRD patterns shown in Fig. S1, sulfurization temperatures above 1123 K were sufficient for the formation of single-phase $Sm_2Ti_2S_2O_5$. However, as shown in Fig. 3a, the optimal preparation temperature for H_2 evolution was 1223 K for both 5% Mg-doped and 1% Ag-modified samples. In contrast, the influence of the electron donor concentration (S^{2-} and SO_3^{2-}) on the activity of 5% Mg- or 1% Ag-modified samples was completely the opposite, as shown in Fig. 3b. With increasing electron donor concentration, the H_2 evolution rate of a 1% Ag-modified sample was enhanced, but the value decreased for a 5% Mg-modified sample. In summary, the maximum rates of Mg- or Ag-modified photocatalysts were obtained for 5%Mg–$Sm_2Ti_2S_2O_5$-1223 (275 μmol h^{-1}) and 1%Ag–$Sm_2Ti_2S_2O_5$-1223 (312 μmol h^{-1}).

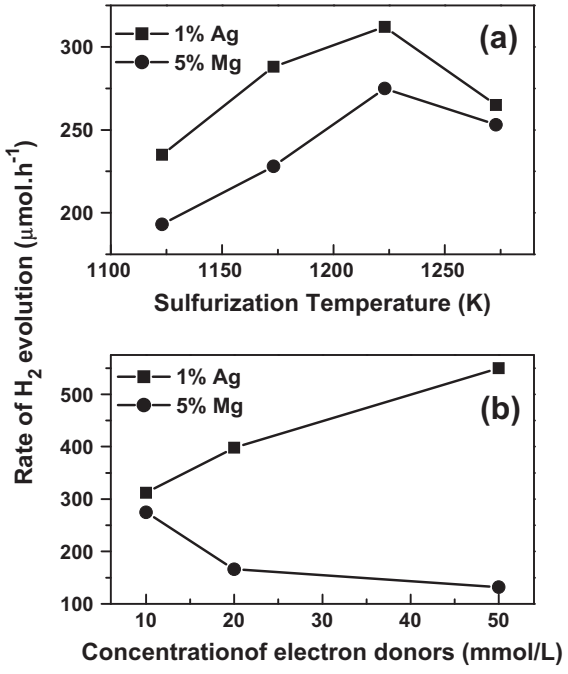

Fig. 3. Effects of preparation and reaction conditions on photocatalytic H_2 evolution over 1% Ag- or 5% Mg-modified $Sm_2Ti_2S_2O_5$: (a) sulfurization temperature and (b) concentration of Na_2S-Na_2SO_3 solution.[a] Reaction conditions: catalyst, 0.2 g (1 wt.% Rh cocatalyst); aqueous Na_2S–Na_2SO_3 solution (400 mL); light source, 450 W Hg lamp with an $NaNO_2$ (2 M) solution filter ($\lambda > 400$ nm).[a] The photocatalysts were sulfurized at 1223 K for 1 h.

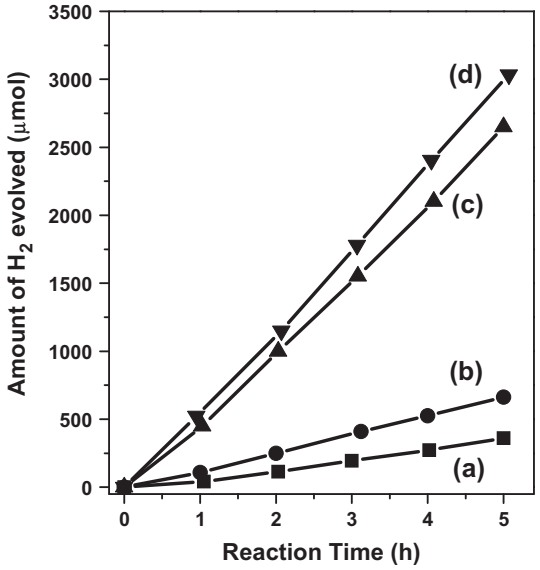

Fig. 4. Typical times for H_2 evolution on various photocatalysts: (a) $Sm_2Ti_2S_2O_5$-1223, (b) 5%Mg–$Sm_2Ti_2S_2O_5$–1223, (c) 1%Ag–$Sm_2Ti_2S_2O_5$-1223, and (d) 1%Ag5%Mg–$Sm_2Ti_2S_2O_5$-1223. Reaction conditions: catalyst, 0.2 g (1 wt.% Rh cocatalyst); aqueous Na_2S–Na_2SO_3 solution (400 mL, 0.05 M); light source, 450 W Hg lamp with an $NaNO_2$ (2 M) solution filter ($\lambda > 400$ nm).

Fig. 4 exhibits the time courses of H_2 evolution from a 0.05 M Na_2S–Na_2SO_3 solution for the optimized samples. It was found that the rate of H_2 evolution became constant after an initial induction period. The reactions were also tested in the dark, but no reaction occurred. The steady rates of H_2 evolution over $Sm_2Ti_2S_2O_5$-1223, 5%Mg–$Sm_2Ti_2S_2O_5$-1223, and 1%Ag–$Sm_2Ti_2S_2O_5$-1223 were calculated to be ca. 88, 136, and 550 μmol h^{-1}, respectively. The H_2 evolution rate was further improved using both 5% Mg and 1% Ag additives (1%Ag5%Mg–$Sm_2Ti_2S_2O_5$-1223), which had a stable value of 630 μmol h^{-1}, about 7 times that of the unmodified sample.

It should be pointed out that the H_2 evolution rate on the 1%Ag–$Sm_2Ti_2S_2O_5$ in this study is not as high as that in our previous work [17], because we adopted different deposition method of rhodium. In this study, the rhodium was in situ photodeposited, while it was impregnated and reduced by hydrogen at 573 K for 1 h in our previous work. The different metal deposition method usually affects its size, morphology, and dispersion on the surface of photocatalyst, finally leading to distinct catalytic performances. The exact reason on this point is under investigation and will be reported elsewhere.

3.2.2. Characterization of photocatalysts

Structural characterizations were carried out on the unmodified and metal-modified samples with optimal photocatalytic activity, such as 1%Ag–$Sm_2Ti_2S_2O_5$-1223 and 5%Mg–$Sm_2Ti_2S_2O_5$-1223. First, XRD patterns and SEM images of the optimized samples with and without metal additives were compared. As shown in Figs. S2 and S3, no noticeable difference in morphology, crystallinity, or particle size could be identified.

The valence states of the Ag- and Mg species were investigated by XPS. For the Ag-modified sample, earlier work using high-resolution transmission electron microscopy, XPS, and X-ray absorption spectroscopy revealed that the Ag species are deposited on $Sm_2Ti_2S_2O_5$ as Ag_2S nanoparticles with diameters of a few tens of nanometers [17]. Different from the clear observation of Ag_2S species on the 1%Ag–$Sm_2Ti_2S_2O_5$-1223 sample, no obvious particles

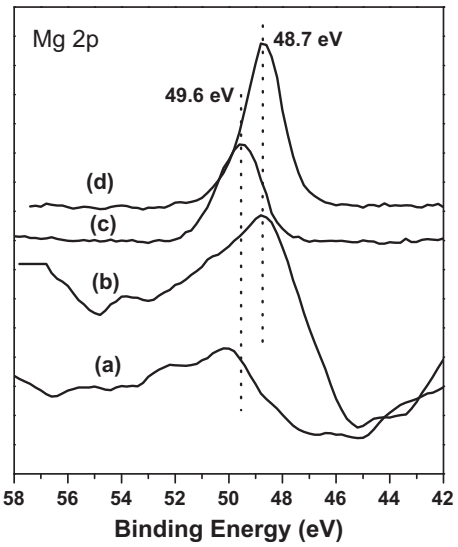

Fig. 5. Mg 2p XPS spectra of various samples: (a) 5%Mg–$Sm_2Ti_2S_2O_5$-1223, (b) 5%Mg–$Sm_2Ti_2O_7$, (c) MgS, and (d) MgO.

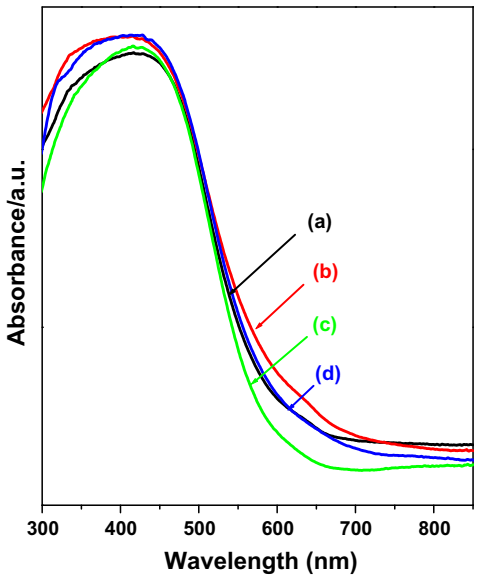

Fig. 6. UV–visible diffuse reflectance spectra of (a) $Sm_2Ti_2S_2O_5$-1223, (b) 1% Ag–$Sm_2Ti_2S_2O_5$-1223, (c) 5%Mg–$Sm_2Ti_2S_2O_5$-1223, and (d) 1%Ag5% Mg–$Sm_2Ti_2S_2O_5$-1223.

assigned to any Mg species can be observed on the TEM image of 5%Mg–$Sm_2Ti_2S_2O_5$-1223, which is given in Fig. S4, together with that of $Sm_2Ti_2S_2O_5$-1223 as comparison. Fig. 5 shows the Mg 2p XPS spectrum of the 5%Mg–$Sm_2Ti_2S_2O_5$-1223 sample, along with those of the oxide precursor, MgS, and MgO for references. The XPS peak of the sample was relatively broad and was located at the highest binding energy position of all samples examined, although the peak intensity was very weak, primarily because of the low concentration of Mg. This result indicates that the Mg species interacts with the sulfur species in a complicated manner. The coordination numbers of Sm^{3+} and Ti^{4+} in $Sm_2Ti_2S_2O_5$ are 12 and 6, respectively, and the ionic radii are Sm^{3+} (109.8 pm) and Ti^{4+} (74.5 pm) [30]. Since it is difficult for Mg^{2+} ions to have a 12-coordinated state and the ionic radius of Mg^{2+} (86 pm) is close to Ti^{4+} with a coordination number of 6, it is most likely that the Mg species was incorporated into the crystal lattice of $Sm_2Ti_2S_2O_5$. This is, however, inconsistent with the XRD results, which showed almost no change in the peak positions. Presumably, the low concentration of Mg and the similar ionic size are responsible for this apparent contradiction. On the other hand, as described in a previous paper [17], Ag^+ ions (129 pm, 6-coordinated state) are too large to be incorporated, and the Ag species migrated during the sulfurization process and became deposited on the $Sm_2Ti_2S_2O_5$ as Ag_2S nanoparticles.

The UV–Vis spectra shown in Fig. 6 confirm that the parent sample had an absorption edge of ca. 600 nm, but with an increased background absorption at wavelengths longer than 600 nm. The former was due to the band gap transition of $Sm_2Ti_2S_2O_5$, while the latter can be ascribed to the existence of a small amount of Ti^{3+} species in the sample, resulting from the reduction in Ti^{4+} by exposure to H_2S [16]. Compared with the parent catalyst, samples with metal modification had a similar absorption edge but different levels of background absorption. The absorption of 1%Ag–$Sm_2Ti_2S_2O_5$-1223 below 700 nm was larger to some extent, likely due to additional absorption from the Ag_2S [17]. However, the absorption background above 700 nm decreased, indicating that the Ag additive prevented the formation of Ti^{3+} species somewhat. For the 5%Mg–$Sm_2Ti_2S_2O_5$-1223 sample, an obvious decrease in the absorption background was observed, indicating that the formation of Ti^{3+} species was effectively inhibited. This idea was further supported by the observation that the background absorption of $Sm_2Ti_2S_2O_5$ tended to decrease with increasing Mg content (Fig. S5). The absorption curve of a sample modified with both 1% Ag and 5% Mg showed a combination of both of the metal modification effects.

Fig. 7 shows photoluminescene spectra of the same samples. Unmodified $Sm_2Ti_2S_2O_5$ generated luminescence centered at 827 nm upon excitation with 400 nm photons. Modification of $Sm_2Ti_2S_2O_5$ with either Ag or Mg resulted in a reduction in photoluminescence intensity without changing the maximum wavelength. It is interesting that the photoluminescence intensity at 827 nm was further reduced in the 1%Ag5%Mg–$Sm_2Ti_2S_2O_5$-1223 sample. This reduced photoluminescence intensity suggests that Ag and Mg modification effectively suppresses the generation of defect sites that act as electron-hole recombination centers and that the Mg doping leads to a more pronounced reduction in photoluminescene intensity.

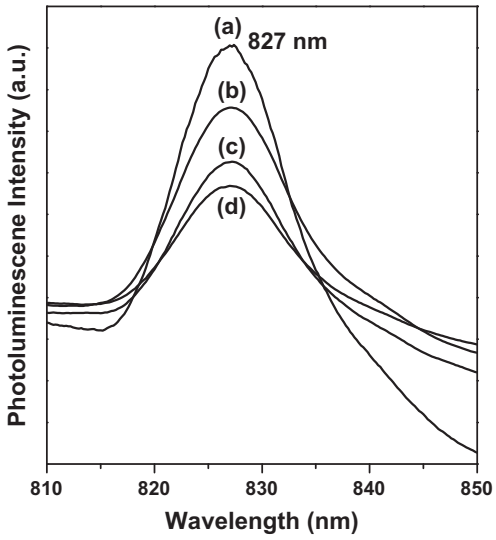

Fig. 7. Photoluminescence spectra measured at 77 K with 400 nm excitation: (a) $Sm_2Ti_2S_2O_5$-1223, (b) 1%Ag–$Sm_2Ti_2S_2O_5$-1223, (c) 5%Mg–$Sm_2Ti_2S_2O_5$-1223, and (d) 1%Ag5%Mg–$Sm_2Ti_2S_2O_5$-1223.

Based on the photocatalyic results shown in Table 2 and Figs. 3 and 4, we can draw the following conclusions: (i) 1% Ag or 5% Mg modification can efficiently promote H_2 evolution and (ii) the H_2 evolution rate is strongly related to both the concentration of the Na_2S–Na_2SO_3 electron donor solution and the preparation temperature. With a low concentration of electron donors (0.01 M), the H_2 evolution rate on both 5% Mg and 1% Ag-modified photocatalysts was approximately three times that of an unmodified sample (Table 2). On the other hand, using highly concentrated electron donors (0.05 M), the stable H_2 activities of the 5% Mg and 1% Ag-modified powders became 1.5 and 6 times that of the unmodified sample, respectively (Fig. 4).

The photocatalytic performance of a given material can be influenced by various factors, such as crystallinity, morphology, particle size, and specific surface area [3,4]. The similar crystallinity, morphology, and particle size (specific surface area) of the unmodified and the metal-modified samples, as indicated by the XRD and SEM results (Figs. S2 and S3), suggest that another explanation is required for the remarkable promotion of H_2 evolution rate. The reduction in the defect density in the Ag- or Mg-modified samples, as demonstrated by the UV–Vis and photoluminescene spectra, might be regarded as evidence of their enhanced photocatalytic activity. However, this cannot explain the variation of the effects of Ag and Mg modification on the activity under different electron donor concentrations.

Since photocatalytic H_2 evolution is initiated by the oxidation of electron donors by photogenerated holes in the valence band of the photocatalyst, the H_2 evolution rate in the half-reaction is usually limited by the hole-scavenging rate. $Sm_2Ti_2S_2O_5$ is an n-type semiconductor, so it is possible to monitor the photooxidation reaction occurring on its surface using a photoelectrochemical technique. Photoelectrochemical measurements were taken using $Sm_2Ti_2S_2O_5$-1223, 1%Ag–$Sm_2Ti_2S_2O_5$-1223, 5%Mg–$Sm_2Ti_2S_2O_5$-1223, and 1%Ag5%Mg–$Sm_2Ti_2S_2O_5$-1223 photoanodes under intermittent irradiation by visible light in a 0.01 M Na_2S–Na_2SO_3 solution. Fig. 8 shows the resulting current–voltage curves, in which all electrodes generated anodic photocurrents based on the oxidation of S^{2-} and SO_3^{2-} ions. However, Mg and Ag additives had opposing influences on the photocurrent. Compared with an $Sm_2Ti_2S_2O_5$ electrode, the Ag-modified electrode demonstrated a significantly increased photocurrent, while the photocurrent was greatly suppressed in the Mg-doped electrode. The photocurrent generated from the 1%Ag5%Mg–$Sm_2Ti_2S_2O_5$-1223 electrode was between those of the unmodified and Ag-modified electrodes. Therefore, the oxidation efficiency of S^{2-} and SO_3^{2-} ions on the surfaces of these electrodes decreased in the order: 1%Ag–$Sm_2Ti_2S_2O_5$ > 1%Ag5%Mg–$Sm_2Ti_2S_2O_5$ > $Sm_2Ti_2S_2O_5$ > 5%Mg–$Sm_2Ti_2S_2O_5$.

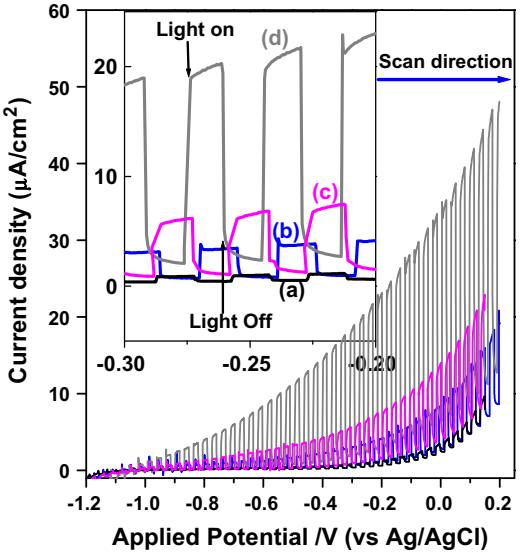

Fig. 8. Current–voltage curves of various electrodes under intermittent visible irradiation in an Na_2S–Na_2SO_3 solution: (a) 5%Mg–$Sm_2Ti_2S_2O_5$-1223, (b) $Sm_2Ti_2S_2O_5$-1223, (c) 1%Ag5%Mg–$Sm_2Ti_2S_2O_5$-1223, and (d) 1% Ag–$Sm_2Ti_2S_2O_5$-1223.

Concerning the different influence of concentration of electron donors on the Mg- or Ag-modified sample observed in Fig. 3b, the main reason can be attributed to their distinct photooxidation efficiency and the flat band potential of $Sm_2Ti_2S_2O_5$, which was found to be independent on pH values in our previous work [15]. The band positions of $Sm_2Ti_2S_2O_5$ as a function of pH values are described in Fig. S6, from which we can deduce that the position of the conduction band becomes close to water reduction potential with increasing pH. It means that the increased pH environment is unfavorable for the reduction of proton due to the decreased driving force. In this work, the pH values of reaction solutions were increased from ca.12.42 to 13.26, when the concentration of Na_2S–Na_2SO_3 was increased from 0.01 to 0.05 M. Together with the inhibition of photooxidation efficiency on the Mg-modified sample indicated in Fig. 8, the photocatalytic H_2 performance was thus decreased with increased concentration of electron donors. Ag modification, however, can enhance the photooxidation efficiency. Highly concentrated electron donors will provide more opportunity for the adsorption and activation of S^{2-} and SO_3^{2-} anions and result in more efficient photooxidation. Thus the rate of H_2 evolution on the Ag-modified sample was integrally enhanced with increasing concentration of electron donors, although which decreased the driving force of carriers.

The rate of H_2 evolution in this study was mainly determined by two factors: the defect density of catalyst and the photooxidation efficiency of the electron donors. The addition of 5% Mg to $Sm_2Ti_2S_2O_5$ can effectively reduce the density of defects, thereby enhancing the number of photogenerated carriers available for surface chemical reactions. However, this addition has a negative effect on the photooxidation of electron donors. In contrast, 1% Ag additive reduced the density of defects, but promoted photooxidation. The density of defects can be further reduced by co-modification with 1% Ag and 5% Mg. Overall, the order of H_2 evolution rate was as follows: 1%Ag5%Mg–$Sm_2Ti_2S_2O_5$ > 1%Ag–$Sm_2Ti_2S_2O_5$ > 5%Mg–$Sm_2Ti_2S_2O_5$ > $Sm_2Ti_2S_2O_5$.

Finally, the apparent quantum efficiency on the 1%Ag5%Mg–$Sm_2Ti_2S_2O_5$-1223 sample with an in situ photo-deposited Rh as cocatalyst was measured in a 0.05 M Na_2S–Na_2SO_3 solution. It was calculated as 5.8% at 440 nm.

4. Conclusions

Modification with metal additives was shown to be an effective approach for improving the photocatalytic H_2 evolution rate of oxysulfide $Sm_2Ti_2S_2O_5$ under visible light irradiation. The influence of Ag or Mg additives on the structure of the photocatalyst and the mechanism of H_2 evolution rate promotion were determined on the basis of detailed characterization and photoelectrochemical measurements of the photocatalysts. The addition of silver ions led to the formation of Ag_2S nanoparticles that were intimately coupled with the $Sm_2Ti_2S_2O_5$ and promoted oxidation by valance band holes. The heterojunction formed between Ag_2S and $Sm_2Ti_2S_2O_5$ and promotion of oxidation by hole scavengers were the primary reasons for the enhanced photocatalytic activity of the Ag–$Sm_2Ti_2S_2O_5$ powder. On the other hand, magnesium ions were mainly incorporated into the photocatalyst, preventing the formation of Ti^{3+} species as defects, and the oxidation process was significantly inhibited. The apparent quantum efficiency on the optimal

sample was measured as 5.8% at 440 nm. Enhanced H_2 evolution activity may be expected from co-modification with Ag and another metal that can reduce the density of defects without hindering the oxidation ability. Possible alternatives to magnesium for this purpose are currently under investigation.

Acknowledgments

This work was supported by the Global Center of Excellence (GCOE) Program for Chemistry Innovation through Cooperation of Science and Engineering and the Research and Development in a New Interdisciplinary Field Based on Nanotechnology and Materials Science programs of the Ministry of Education, Culture, Sports, Science and Technology (MEXT) of Japan. One of the authors (K. M.) gratefully acknowledges the support of Nippon Sheet Glass Foundation for Materials Science and Engineering. Acknowledgment is also extended to the KAITEKI Institute, Inc., for financial support. The authors also thank Prof. S.T. Oyama for useful discussion.

Appendix A. Supplementary material

Supplementary data associated with this article can be found, in the online version, at doi:10.1016/j.jcat.2011.01.027.

References

[1] J.S. Lee, Catal. Surv. Asia 9 (2005) 217.
[2] R. Abe, K. Sayama, H. Sugihara, J. Phys. Chem. B 109 (2005) 16052.
[3] K. Maeda, K. Domen, J. Phys. Chem. C 111 (2007) 7851.
[4] A. Kudo, Y. Miseki, Chem. Soc. Rev. 38 (2009) 253.
[5] F.E. Osterloh, Chem. Mater. 20 (2008) 35.
[6] K. Maeda, K. Teramura, D.L. Lu, T. Takata, N. Saito, Y. Inoue, K. Domen, Nature 440 (2006) 295.
[7] K. Maeda, M. Higashi, D.L. Lu, R. Abe, K. Domen, J. Am. Chem. Soc. 132 (2010) 5858.
[8] R. Abe, H. Takami, B. Ohtani, J. Am. Chem. Soc. 130 (2008) 7780.
[9] X. Zong, H.J. Yan, G.P. Wu, G.J. Ma, F.Y. Wen, L. Wang, C. Li, J. Am. Chem. Soc. 130 (2008) 7176.
[10] H.J. Yan, J.H. Yang, G.J. Ma, G.P. Wu, X. Zong, Z.B. Lei, J.Y. Shi, C. Li, J. Catal. 266 (2009) 165.
[11] A. Kasahara, K. Nukumizu, G. Hitoki, T. Takata, J.N. Kondo, M. Hara, H. Kobayashi, K. Domen, J. Phys. Chem. A 106 (2002) 6750.
[12] K. Kamata, K. Maeda, D. Lu, Y. Kako, K. Domen, Chem. Phys. Lett. 470 (2009) 90.
[13] G. Hitoki, A. Ishikawa, T. Takata, J.N. Kondo, M. Hara, K. Domen, Chem. Lett. 31 (2002) 736.
[14] L. Yuliati, J.H. Yang, X. Wang, K. Maeda, T. Takata, M. Antonietti, K. Domen, J. Mater. Chem. 20 (2010) 4295.
[15] A. Ishikawa, T. Takata, J.N. Kondo, M. Hara, H. Kobayashi, K. Domen, J. Am. Chem. Soc. 124 (2002) 13547.
[16] A. Ishikawa, Y. Yamada, T. Takata, J.N. Kondo, M. Hara, H. Kobayashi, K. Domen, Chem. Mater. 15 (2003) 4442.
[17] F.X. Zhang, K. Maeda, T. Takata, K. Domen, Chem. Commun. 46 (2010) 7313.
[18] K. Maeda, A. Xiong, T. Yoshinaga, T. Ikeda, N. Sakamoto, T. Hisatomi, M. Takashima, D. Lu, M. Kanehara, T. Setoyama, T. Teranishi, K. Domen, Angew. Chem. Int. Ed. 49 (2010) 4096.
[19] K. Maeda, K. Teramura, N. Saito, Y. Inoue, K. Domen, J. Catal. 243 (2006) 303.
[20] H. Kato, K. Asakura, A. Kudo, J. Am. Chem. Soc. 125 (2003) 3082.
[21] C.C. Hu, H.S. Teng, J. Catal. 272 (2010) 1.
[22] O. Rosseler, M.V. Shankar, M.K.L. Du, L. Schmidlin, N. Keller, V. Keller, J. Catal. 269 (2010) 179.
[23] R. Niishiro, R.A. Konta, H. Kato, W.J. Chun, K. Asakura, A. Kudo, J. Phys. Chem. C 111 (2007) 17420.
[24] X. Yang, C. Cao, K. Hohn, L. Erickson, R. Maghirang, D. Hamal, K. Klabunde, J. Catal. 252 (2007) 296.
[25] D.W. Hwang, H.G. Kim, J.S. Lee, J. Kim, W. Li, S.H. Oh, J. Phys. Chem. B 109 (2004) 2093.
[26] K. Takanabe, T. Uzawa, X.C. Wang, K. Maeda, M. Katayama, J. Kubota, A. Kudo, K. Domen, Dalton Trans. 45 (2009) 10055.
[27] M. Takeuchi, H. Yamashita, M. Matsuoka, M. Anpo, T. Hirao, N. Itoh, N. Iwamoto, Catal. Lett. 67 (2000) 135.
[28] A.W. Xu, Y. Gao, H.Q. Liu, J. Catal. 207 (2002) 151.
[29] X.C. Wang, J.C. Yu, H.Y. Yip, L. Wu, P.K. Wong, S.K. Lai, Chem. Eur. J. 11 (2005) 2997.
[30] R.D. Shanon, Acta Cryst. A32 (1976) 751.